Tellus (2001), 53A, 112–128
Printed in UK. All rights reserved

TELLUS
ISSN 0280–6495

Observed and modelled sea-ice drift response to wind forcing in the northern Baltic Sea

By J. UOTILA*, *Finnish Institute of Marine Research, P.O. Box 33, FIN-00931, Helsinki, Finland*

(Manuscript received 17 January 2000; in final form 11 May 2000)

ABSTRACT

The wind dependence of sea-ice motion was studied on the basis of ice velocity and wind observations, and weather model output. The study area was a transition zone between open water and the ice-covered ocean in the northern Baltic Sea. In the centre of the basin the sea-ice motion was highly wind-dependent and the linear relationship between the wind and the drift velocities explained 80% of the drift's variance. On the contrary, the wind-drift dependence was low near the coast. The wind-drift coherence was significant over a broader frequency range in the central part of the basin than for the coastal drift. The ice motion was simulated by a numerical model forced with five types of wind stress and with two types of current data, and the outcome was compared with the observed buoy drift. The wind and the wind-induced surface current were the main factors driving the ice in the basin's centre, while internal ice stresses were of importance in the shear zone near the fast ice edge. The best wind forcing was achieved by applying a method dependent on atmospheric stability and ice conditions. The average air–ice drag coefficient was 1.4×10^{-3} with the standard deviation of 0.2×10^{-3}. The improvement brought about by using an accurate wind stress was comparable with that achieved by raising the model grid resolution from 18 km to 5 km.

1. Introduction

The ice-covered sea surface forms a complex boundary between the atmosphere and the underlying ocean. The sea ice strongly modifies the air-sea energy exchange, especially in winter when relatively cold air lies over a warm ocean. In these conditions, even small open water fractions are of importance. Accordingly, it is vital to know the sea-ice condition reliably when estimating the regional energy balance of ice-covered oceans. The wind is usually the most important forcing factor for the sea-ice drift, especially when the ice concentration is low. In high concentration conditions, usually near the fast-ice zone, internal ice stresses may play a significant role in modifying the sea-ice dynamics. In addition, sea-surface currents affect the motion of sea ice.

* e-mail: uotila@fimr.fi

Several wind-drift studies have been published in recent years, for example by Kottmeier and Sellmann (1996), Vihma et al. (1996), Geiger et al. (1998), Thomas (1999) and Uotila et al. (2000) on the basis of buoy observations from the Arctic or Antarctic regions. The wind forcing applied in the analyses has usually been the output of large-scale weather models, and uncertainties and the differences between the applied models may be significant. Thus it is important to be aware of the possible errors in the wind forcing and the parameterization of the momentum flux when modelling sea-ice velocities.

In the Baltic Sea, Leppäranta (1981) investigated the motion and mechanics of pack ice in the Bothnian Bay, and more recently Leppäranta et al. (1998) compared the ice velocity fields derived from satellite imagery with modelled ones. Leppäranta and Omstedt (1990) modelled the drift of a ship in the Bothnian Bay with a coupled ice-ocean model, while Gustafsson et al. (1998) presented a coupled atmosphere–ice–ocean model for the Baltic Sea.

Highly accurate forecasts of ice conditions are important for the northern Baltic Sea, which is frequently navigated by shipping in winter. Accordingly, accurate wind forcing together with a well-suited dynamic ice model are necessary when forecasting the ice conditions. In the Baltic Sea the meteorological observation network is much denser than in the Arctic and especially in the Antarctic, providing a good opportunity to compare the effect of the wind data on the sea-ice modelling results.

In February–March 1998, a comprehensive field experiment was carried out in the northern Baltic Sea. The overall objective of this Baltic Air–Sea–Ice Study (BASIS) was to create and analyze an experimental data set for the optimization and verification of coupled atmosphere–ice–ocean models (Launiainen, 1999). BASIS is a subprogram of the Baltic Sea Experiment (GEWEX/BALTEX). One of the specific objectives covers the investigation of forcing at air–ice and ice–water boundaries, the topic which is addressed in this paper. Another specific objective of BASIS is the modelling of sea-ice dynamics. In the study, this was partly done by simulating the ice drift during the main field experiment and comparing the model outcome with the ice drift observed by buoys. The BASIS data set provided a very good observational base from which to study the wind-drift relationship and compare that with the modelling results.

In Section 2 the data applied in the study is introduced. In Section 3 the relationship between the measured drift and the wind is investigated. In Section 4 a numerical model for the sea ice velocity is presented and the modelled velocities are compared with the observed ones. Finally, in Section 5 some conclusions are drawn from the analysis.

2. Data

2.1. *Ice conditions, concentration and thickness*

The study area was located at the transition zone between the open ocean in the Bothnian Sea and the ice-covered ocean in the Bothnian Bay (Fig. 1). The strait that connects these two basins is relatively shallow and narrow with a complex archipelago. Weak advective exchange can be expected through the strait between the basins (see for example Omstedt, 1990). Near the coasts the land-fast ice connected the archipelago to the main land, while there were drifting pack ice in the central part. The pack ice ridged and rafted against the fast ice mainly in the eastern side and central part, while regions of low ice concentration were opened up in the western side of the basin. The fast-ice thickness was 20–35 cm and the thickness of undeformed pack ice varied from 10 to 40 cm. The complex topography and many ice-types requires a sufficiently high resolution model to resolve the ice motion. On the other hand, the commonly applied ice rheology parameterization follow the continuum approximation of Hibler (1979), which requires many ice floes in a single gridcell. The large ice floes in the Baltic Sea are commonly 1–3 km in diameter (Leppäranta et al., 1998). The BASIS buoys were deployed on ice floes of around 1 km in diameter, which was found to be apparently more than the common size of the ice floes in the region. With the information of ice floe sizes during the BASIS experiment and results of Zhang et al. (1999), it seems that the continuum approximation of Hibler (1979) is not violated by applying the grid size of 5 km. The grid size is still one order of magnitude greater than ordinary floe size.

The ice concentration and thickness were derived from the daily SMHI and FIMR ice charts. Although the overall agreement between the analyses was quite good, the ice thicknesses in particular seemed to have a systematic difference. Occasionally the ice concentrations differed a lot, for example when buoy 5893 was surrounded by open water or a new ice region. In these cases the RADARSAT satellite images were studied. Additionally, mean values of the ice concentration and thickness from the two institutes were applied in such cases. The resolution of the FIMR ice concentration fields was 18.5 km, and that of the SMHI fields was 16.5 km.

2.2. *Sea-ice velocity*

Between 18 and 22 February 1998, six drifting buoys were deployed in the Gulf of Bothnia, five on sea ice floes and one in open water. Two of the buoys were equipped with the Global

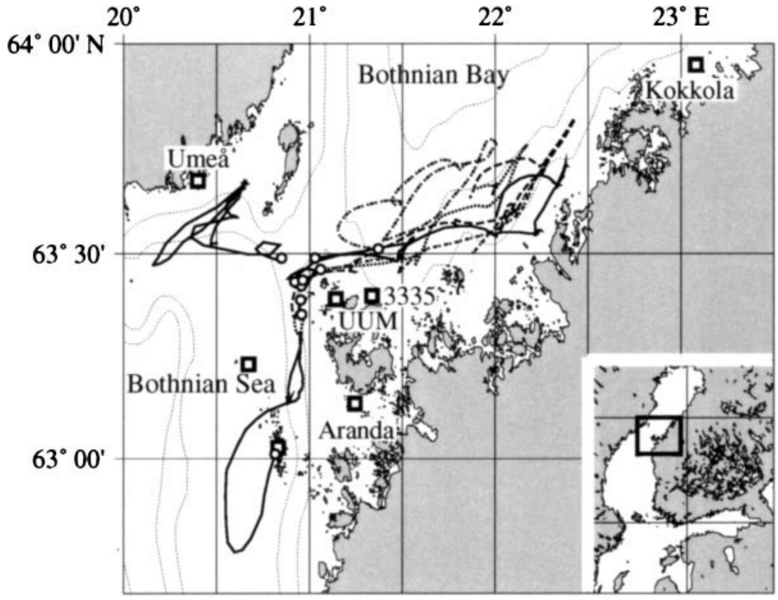

Fig. 1. The drift trajectories (thick lines) and the initial positions (open circles) of the BASIS buoys, and the positions of the nearest meteorological stations (squares). UUM is the Uppsala University weather mast and 3335 is a weather buoy of the University of Hamburg. R/V Aranda was the main observing station of the BASIS experiment. Thin dashed lines give the depth countours with 20 m interval up to 20 m depth.

Positioning System (GPS) receivers, otherwise buoy positions were determined by the CLS Argos system. The accuracy of the GPS was of the order of 100 m, while the accuracy of CLS Argos was within the range of 100 to 700 m, typically 200 metres. Another buoy with a 4 m high meteorological mast was deployed on fast ice on 18 February, but the ice broke up on 24 February and the buoy began to drift. Locations of this buoy were also included in the study. The trajectories of the drifters during the experiment are presented in Fig. 1.

The buoy positions determined by Argos were interpolated at three-hourly intervals, while GPS positions were interpolated hourly. The higher accuracy of the GPS locations made possible a reliable interpolation of the positions more frequently. The buoy positions were interpolated with a method known as 'Kriging', as described by Hansen and Herman (1989) and Hansen and Poulain (1996), who applied the method for open ocean drifters. Uotila et al. (2000) adapted the method to sea ice drifters in the Weddell Sea. One benefit of the method is that it provides individual error estimates for the quantity at each interpolated point. Knowledge of the accuracy of interpolated velocities, e.g., due to gaps in the original non-interpolated time series is thus obtained. The sea ice velocities were then calculated from the interpolated positions.

One GPS-drifter and one Argos-drifter functioned for only a few days, and the velocity time series from these were considered to be too short for the most part of the study. One GPS-drifter (Argos ID 5893) functioned between 19 and 26 February 1998, and produced high-quality hourly locations. The two drifters on ice floes with Argos positioning, 7199 and 9868, functioned from 18 February until 5 March and 20 May 1998, respectively. These buoys drifted near GPS-drifter 5893, but closer to the fast ice. The open water drifter (7198) functioned until 16 March 1998, and gave some approximate information about the surface currents during the experiment. There was no drogue installed on 7198, and thus its motion did not represent the pure ocean current: the windage, i.e., the direct effect of wind on the buoy hull, and wave effects may have been significant. However the mean ratio between the 7198 speed and the geostrophic wind speed was 1.2%, which is about the same than observed speed ratios for drifters with a drogue at a depth of 5 m in the Bothnian Sea in November, 1991 (Uotila et al., 1995). The drift of the buoys was compared with sea level data in Section 4 to see how the drift followed the barotropic ocean currents. As a whole the combined data from the four buoys 5893, 7198, 7199 and 9868 was very suitable for studying the wind-drift relationship and the coastal effects modifying the relationship, and for verification of the dynamic sea ice model.

2.3. *Wind speed and direction*

During the expedition, observations were available from several coastal meteorological stations (Fig. 1). The wind observations were interpolated to the buoy sites. First, the wind at the 10 m level was estimated from the observations made at various heights. The 10 m wind components were then interpolated to the buoy sites, weighting each observation with its inverse distance from the buoy positions. Four meteorological stations were used in the interpolation: Kokkola, Umeå, the meteorological mast of Uppsala University, and buoy 3335 (see Fig. 1).

In addition to the coastal meteorological data, fields from an operational mesoscale analysis system (MESAN) were obtained from the Swedish Meteorological and Hydrological Institute (SMHI). The MESAN fields were estimated by applying meteorological fields from the High Resolution Limited Area Model (HIRLAM) as first guesses and then verifying the fields with surface observations and satellite data (Häggmark et al., 2000). The MESAN fields were calculated at every 3rd hour with a resolution of 11 km in both meridional and zonal directions. The 10 m wind and the geostrophic wind from the atmospheric pressure gradient were calculated at the buoy sites from the MESAN fields. The gradient components were derived from atmospheric pressure subfields of 4 grid-point values around the buoy locations. The observations of the BASIS stations were not included in MESAN, and therefore winds interpolated to the buoy sites from these two sources of data were mutually independent.

The weather conditions during the BASIS field expedition were rather variable because of passing cyclones, which crossed the research area from west to east. The 10-m wind time series in Fig. 2a is characterized by varying speeds of up to 20 m/s following largely the pattern of the geostrophic wind. Westerly winds prevailed, but the wind turned to blow from the north after the cyclones had passed eastwards over the area on 24 February, and on 1 and 5 March 1998 (Fig. 2b). Before 5 March cyclones crossed to the north of the research area, but on that date a cyclone passed to the south of the area, causing winds to blow from the east and south. The weather was generally mild during the expedition with large temperature fluctuations (Fig. 2c). During the cold air outbreak on 24 February, however, the air temperature rapidly decreased from around 0°C to almost -15°C. Following this, the temperature returned to its initial level with the prevalence of westerly winds. On 28 February, a cyclone was centred just north of the research site over the Bothnian Bay, causing cold air originating in the north to flow over the area. Due to this, the temperature gradually decreased until 2 March.

The MESAN 10 m wind was about 42% of the geostrophic wind, turning on average 37° left of it. The BASIS wind was 48% of the geostrophic wind, deviating on average 33° left. The difference in speed ratio can be explained by the fact that the MESAN wind represented average values over a grid square, while the BASIS wind was derived from point observations. The roughness of a grid square that was partly over land, included the higher roughness of the land areas, and further reduced the surface wind from the geostrophic wind speed. To verify this, the speed ratio and turning between the MESAN surface and geostrophic wind were calculated for a point in the middle of the Bothnian Sea, i.e., at 62°N., 20°E. The speed ratio now increased to 53%.

The agreement between the BASIS and MESAN winds was fairly good. The correlation coefficient between the vector time series of the winds was 0.95 (between 0.92 and 0.97 at the 95% confidence level). The BASIS and the MESAN winds correlated with the geostrophic wind with coefficients of 0.76 and 0.73, respectively. In addition, daily HIRLAM analyses (at 12 UTC) and forecasts every 6 h from the Finnish Meteorological Institute (FMI) were utilized when the numerical ice model runs were made in Section 4. The HIRLAM wind was originally input to the Finnish Institute of Marine Research (FIMR) operational

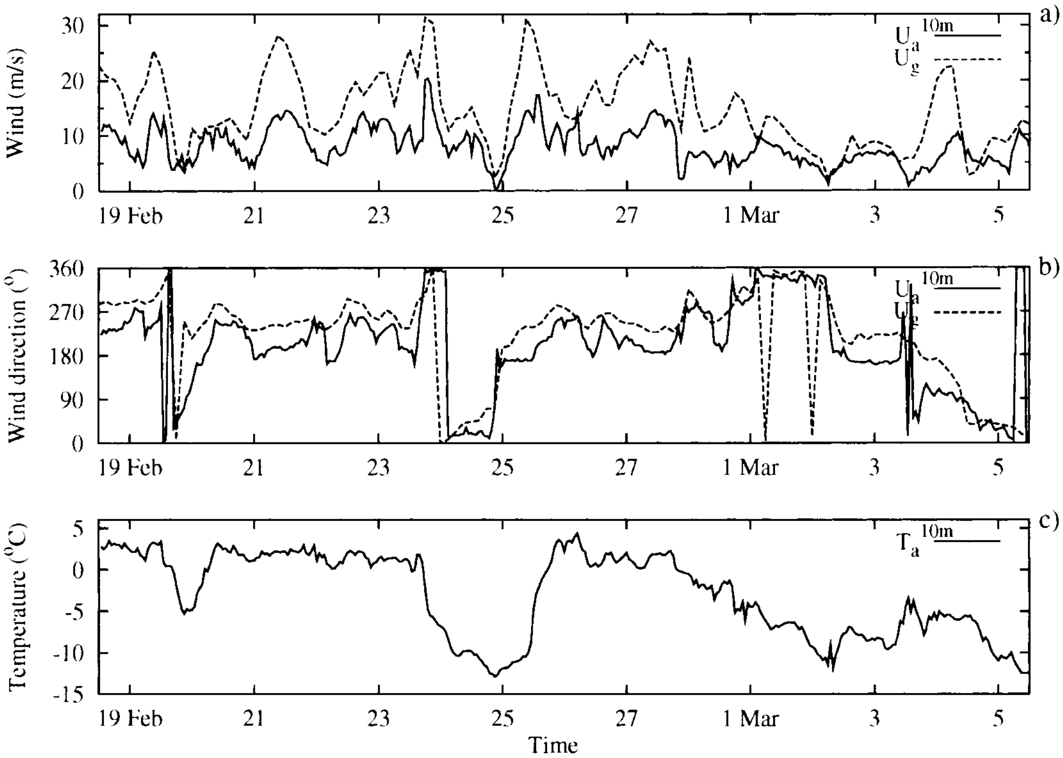

Fig. 2. Time series of (a) the 10-m wind and the geostrophic wind speeds, (b) and directions and (c) the air temperature at a height of 10 m during the BASIS main field expedition in 1998 as measured at the location of R/V Aranda.

ice model when forecasting ice conditions in the Baltic Sea.

3. Wind-drift relationship

The drift speed of the buoys followed the general weather patterns, although internal ice stress close to the coastline reduced the wind-drift dependence. Accordingly, it is important to include the ice concentration and thickness into the analysis. A closer look at the drift of the three buoys is presented in Fig. 3. The buoys drifted mostly in the same ice field and the differences in their motion were due to the differences in the ice movement near the coast and the open ocean. The drift period was divided into subperiods characterized by the various wind and ice conditions. During the first days of the drift, between 19 and 23 February, the 3 buoys drifted northeast, forced by the winds from the southwest (Figs. 4 and 2). In Fig. 4a, time series of the sea-ice drift speed observed by the buoys are presented. The speed varied a lot, up to a maximum of 0.7 m/s. The ice concentration at the buoy sites was relatively low (Fig. 4c). In addition, some periodic motion near the inertial frequency occurred, a fact especially evident for buoy 5893, which drifted furthest from the coast. This motion could not be explained by the wind and was probably connected with the sea surface currents (see Subsection 4.1). Buoys that drifted near the coast (7199, 9868) moved in some cases at a higher speed than the buoy away from the coast (5893).

Between 23 and 25 February, the two buoys nearest the coast (i.e., 7199 and 9868) were stuck close to the fast ice border (Fig. 3). The ice concentration around the third buoy (5893) remained low, (Fig. 4c) and it drifted back to the southwest. At the time the wind blew from the north. On 25 and 26 February, the wind turned again to blow from the southwest, and the buoys drifted

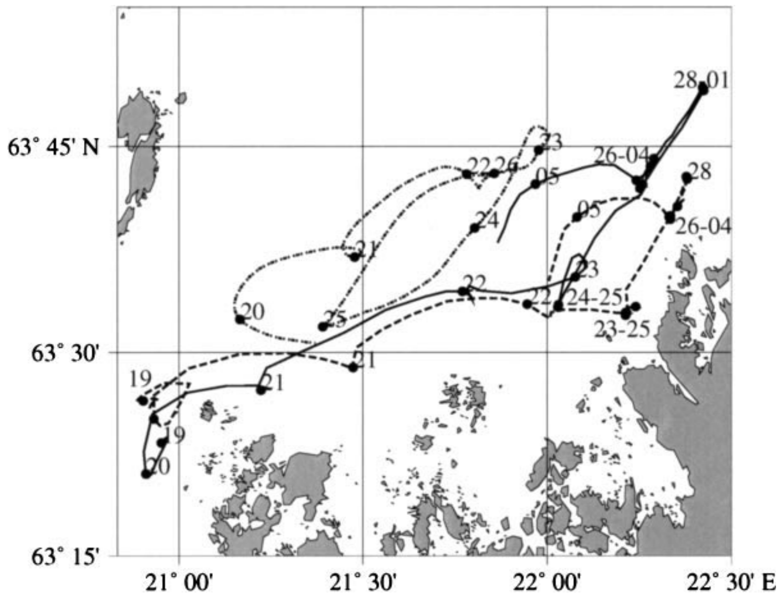

Fig. 3. Trajectories of three drifters between 19 February and 5 March 1998. Daily positions are shown as dots, with dates in February and March. Buoy 9868 is plotted with a solid line, 7199 with a dashed line, and 5893 with a dash–dotted line.

northeast. During these days, the ice concentration around 5893 increased from 50% to compact, and the drifter was destroyed. The two remaining buoys were stuck near the coast, and responded only weakly to the varying winds until 4 March, when seaward winds from the east prevailed and the ice motion was directed towards the open ocean.

3.1. *Linear dependence between the wind and the drift*

By assuming a linear dependence between the complex wind vector $\boldsymbol{u}_{\mathrm{a}}$ and the drift vector $\boldsymbol{u}_i$

$$\boldsymbol{u}_i = s\,\mathrm{e}^{i\varphi}\boldsymbol{u}_{\mathrm{a}} + \boldsymbol{C}, \quad (1)$$

the scaling factor s, turning angle φ, and additive term $\boldsymbol{C}$ were estimated. In (1) $i=\sqrt{-1}$ is the imaginary unit. The linear relationship is physically valid when a thin ice floe has steady-state free drift (see, e.g., Thorndike and Colony (1982)). Temporal changes of these quantities are presented in Fig. 5 for the buoys 5893, 7199, 9868, and reflect the temporal changes in wind, currents and ice conditions, while Table 1 summarises estimates of s, φ and C. The explainability R^2 gives the fraction of the variance of the ice velocity accounted for by the regression model (1).

The highest R^2 and the highest s in Table 1 were obtained for 5893, which drifted mostly in low-concentration ice conditions. The open water drifter 7198 had the second highest s, while the remaining values were on average less than 2%. As discussed in Subsection 2.2, the high s for 7198 may have resulted from the windage effect and waves. The high s for 5893 also gives the impression that the wind-dependent surface currents and waves increased the ratio in the central basin, but did not affect the ice motion so much near the coast (compare to the s of 7199 and 9868). In addition, the C for 5893 was relatively high compared with those of the other drifters in Table 1. The turning angle φ of the ice drifters was about 25° and that of the open water drifter was 30°. These turning angles are comparable with the sea-ice drift in the summer in the Weddell Sea (Martinson and Wamser, 1990; Uotila et al., 2000), with the ice drift in the Bothnian Bay (Leppäranta and Omstedt, 1990), and with the open water drift in the Bothnian Sea (Uotila et al., 1995).

In Fig. 5 the time evolution of the linear model parameters is illustrated. The scaling factors for

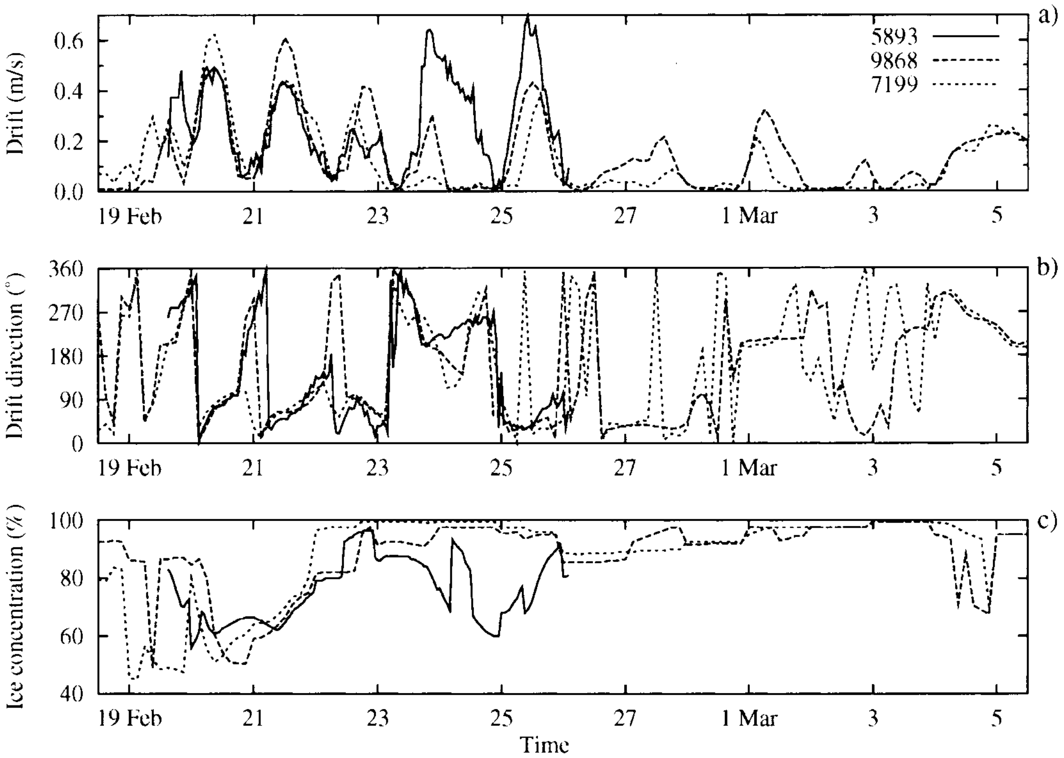

Fig. 4. (a) Drift speeds, (b) directions, and (c) ice concentrations for the drifters 5893, 7199 and 9868.

the three buoys were highest on 19 and 20 February, almost 6%. The drift velocity was turned about 30° to the right of the surface wind and the linear relationship explained the ice motion well. During the first two days the wind-drift correlation was quite high. After that, as the buoys moved closer to the coast and the pack ice was pushed against the fast ice, the scaling factor and the correlation decreased, and the deviation of the turning angle increased.

3.2. *Time-frequency analysis*

The vector coherence and phase were calculated from the drifter velocities and the BASIS wind observations following the method given by Gonella (1972). The method produces the correlations and spectral relations for the clockwise and counterclockwise components between two time series. The vector coherence and the phase between the wind and the drift are presented in Fig. 6. The wind-drift coherence was lower for the buoy that drifted near the coast (7199), and for the open water drifter (7198) than for the most remote buoy from the coast (5893). The coherence for 5893 was significant for the clockwise periods longer than 7 h, i.e., $-3.4 \ldots 0$ cycles per day (cpd), but that for 7199 was significant only between periods of 16 and 30 hours ($-1.5 \ldots -0.8$ cpd). Thus, the wind-drift coherence near the coast was decreased in both at long and the short period regimes. The open water drift was coherent with the wind at periods longer than 30 h and at periods near the inertial motion, i.e., between 11 and 13 h (~ -1.8 cpd). The coherence between the counterclockwise wind and drift components was apparent only at the longest periods of 5893 and 7198, and the phase deviated more than at the clockwise frequencies. The coherence of 5893 is very similar to that observed by Leppäranta and Omstedt (1990). They found that low frequencies were dominated by the wind, whereas high frequencies were dominated by the current. They also observed very high ice-current coherence and a low peak in

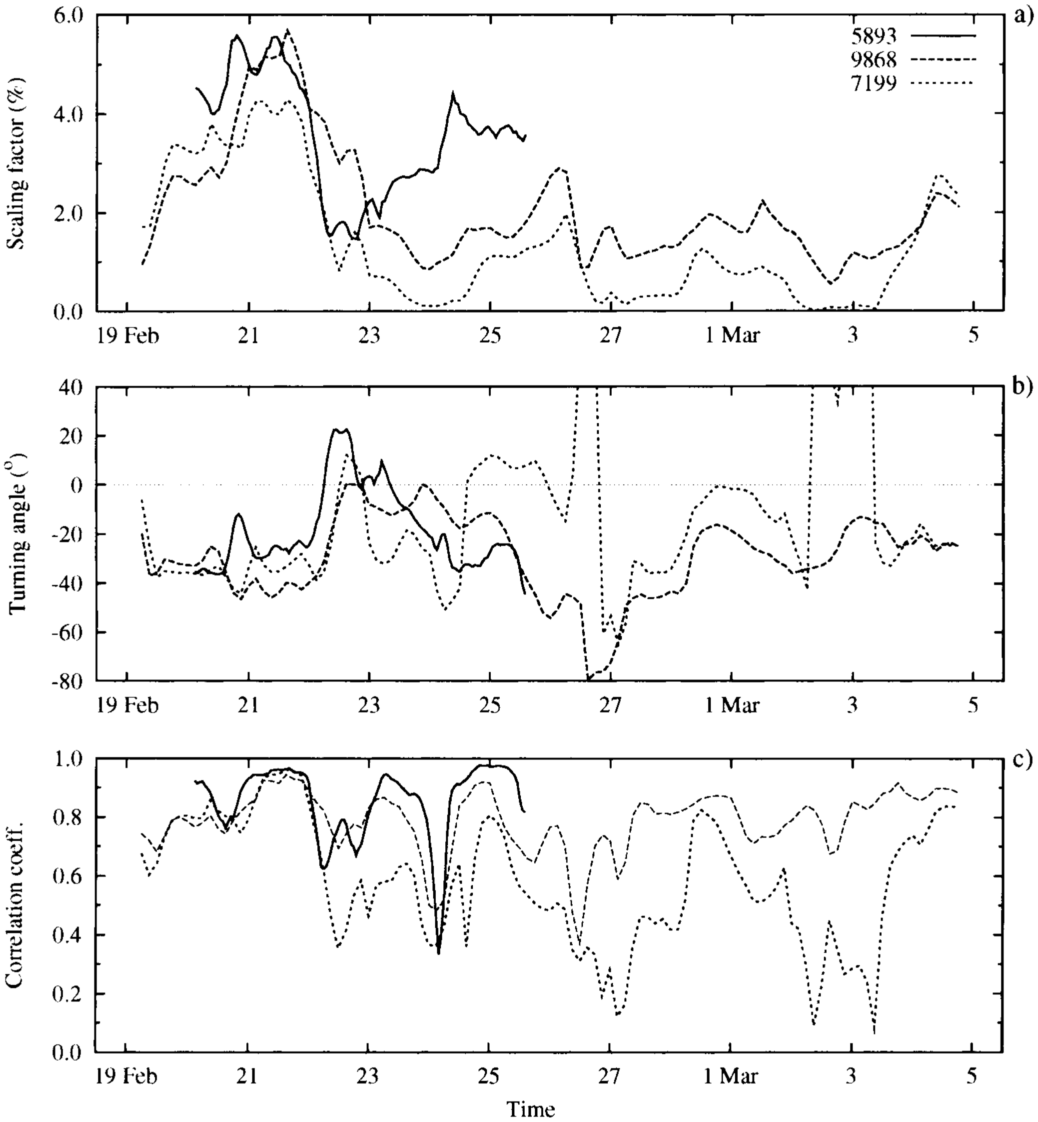

Fig. 5. (a) scaling factor, (b) turning angle, and (c) correlation coefficient between the wind and the drift for the three drifters. A diurnal moving period was chosen for 5893 and 3-day moving periods for 9868 and 7199.

the wind-drift coherence at about -7 cpd (~ 3 h). A similar low peak is apparent in the coherence for 5893 (Fig. 6).

For the period, the clockwise coherence between the wind and the drift was higher than for the counterclockwise component (Fig. 6). The clockwise components of the wind and the drift had more energy, especially at periods between 20 and 48 h, than for the corresponding counterclockwise periods. The energy of the counterclockwise component of the wind was high at periods longer than two days, but then the drift's response to wind was probably restricted by the basin's size and form. Between 23 and 24 February, the counterclockwise wind component had high energy when the surface wind turned from south to west and then to north (Fig. 2b). However, the drift's response to this was quite low, because at that

Table 1. *Scaling factor (s), turning angle (φ), and additive term magnitude (C) between the buoy drift and the interpolated surface wind based on the BASIS meteorological stations; φ is negative if the drift is directed right from the wind; the values in brackets represent the standard deviations of the coefficients, and R^2 gives the ratio of the explained variance of the regression model (1)*

Buoy	s (%)	φ (°)	C (cm/s)	R^2
1154	1.96(0.25)	6(1)	2(4)	0.46
5893	3.25(0.12)	−25(1)	9(3)	0.80
7198	2.49(0.21)	−30(3)	2(2)	0.53
7199	1.25(0.14)	−23(3)	1(3)	0.39
9868	1.76(0.13)	−23(2)	2(2)	0.58
9869	1.68(0.33)	−23(5)	5(5)	0.35

time buoy 5893 drifted in quite compact pack ice, near the shear zone, which decreased the wind-drift response. The lower wind-drift coherence of the counterclockwise component resulted from the wind and ice conditions and basin's dimensions.

4. Drift modelling

We applied a numerical model for the ice velocity, ice concentration, and thickness to simulate the drift of the buoys. The basic equations of the dynamic ice model are the momentum and mass balance equations (Hibler, 1979; Leppäranta, 1981).

$$\rho h(d_t \boldsymbol{u}_i + if\boldsymbol{u}_i) = \tau_a + \tau_w + \nabla \cdot \sigma + \boldsymbol{F}, \tag{2a}$$

$$\partial m/\partial t = -\nabla \cdot (m\boldsymbol{u}_i) + \Phi, \tag{2b}$$

$$m = \rho hA = \rho(h_l + h_r)A. \tag{2c}$$

In eq. (2), ρ is the ice density, h is the mean ice thickness, $\boldsymbol{u}_i$ is the ice velocity vector, f is the Coriolis parameter, τ_a and τ_w are the air–ice and ice-water stresses, $\nabla \cdot \sigma$ is the force due to the gradients in the internal ice stress, and $\boldsymbol{F}$ is the gravitational force due to the sea surface tilt. In addition, m is the ice mass per unit area, Φ is the thermodynamic ice growth rate, A is the ice concentration, and h_l and h_r represent the level and the ridged ice thicknesses. Boldface characters

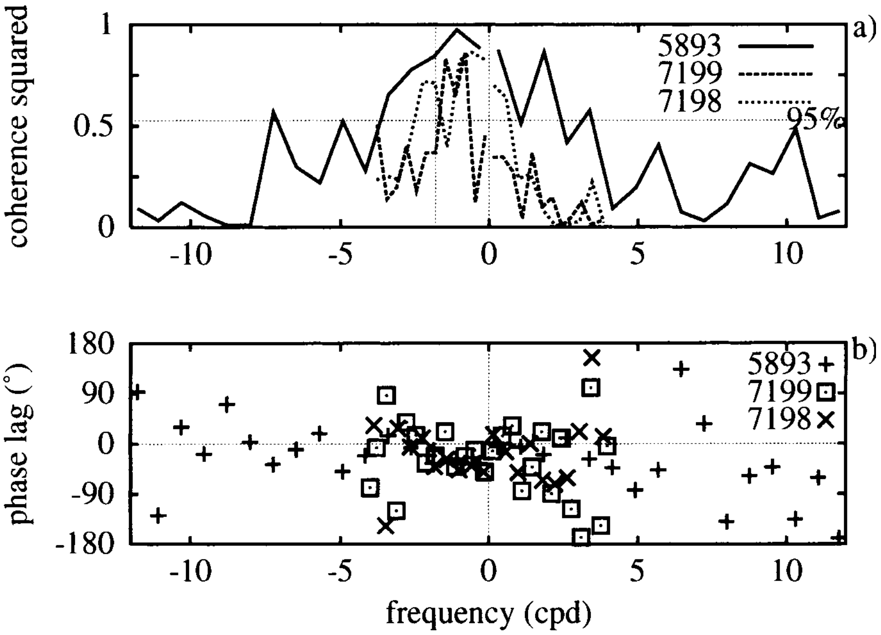

Fig. 6. The wind-drift coherence (a) and phase lag (b) for 5893, 7199, and 7198. Negative frequencies represent a clockwise velocity component, while positive frequencies represent a counterclockwise component. The phase lag is a measure of the phase lead of the rotary component of drift velocity time series with respect to that of wind velocity time series. When the phase lag is positive (negative), the drift vector is directed counterclockwise (clockwise) from the wind. In (a) the vertical dashed line gives the inertial frequency.

represent vectors, and d_t denotes the total derivative operator with respect to time. Here $i=\sqrt{-1}$ is the imaginary unit and (two-dimensional) vectors with magnitude $|\boldsymbol{X}|$ and direction δ have the notation $\boldsymbol{X}=|\boldsymbol{X}|\,\mathrm{e}^{i\delta}$.

The drag terms are parameterized with a quadratic formulation

$$\tau_a = \rho_a C_a |\boldsymbol{u}_a| \boldsymbol{u}_a = \rho_a C_g \,\mathrm{e}^{i\phi} |\boldsymbol{u}_g| \boldsymbol{u}_g, \tag{3a}$$

$$\tau_w = \rho_w C_w \,\mathrm{e}^{i\xi} |\boldsymbol{u}_w - \boldsymbol{u}_i| (\boldsymbol{u}_w - \boldsymbol{u}_i), \tag{3b}$$

where $\boldsymbol{u}_a$ and $\boldsymbol{u}_g$ are the surface wind and geostrophic wind velocities, respectively. In (3b), $\boldsymbol{u}_w$ is the current velocity beneath the ice-water boundary. C_a, C_g, and C_w are the drag coefficients with respect to the surface wind, geostrophic wind, and ocean current beneath the ice–water boundary, respectively; ϕ is the turning angle in the atmospheric boundary layer and ξ is that in the oceanic boundary layer.

We applied two different versions of the numerical ice models in our analysis. The first version was the ice model for the Baltic Sea by Leppäranta and Zhang (1992), which is in operational use in the Finnish Ice Service of FIMR. The model has a spatial grid resolution of 18.5 km, and its time step is 6 h. The internal ice stress is parameterized following the viscous-plastic rheology of Hibler (1979). The second version was introduced by Zhang et al. (1999), having a grid resolution of 5 km, a time step of 15 min, and a more realistic ice rheology with a truncated elliptical yield curve (see Hibler and Schulson, 1997) and more effective calculation routines proposed by Zhang and Hibler, (1997). The truncated elliptical yield curve is a modification of the viscous-plastic elliptical yield curve that eliminates the tensile stress, which is physically realistic at the geophysical scale (for more details, see, for example, Geiger et al., 1998). The FIMR operational ice model set the velocity of fast-ice to zero and ice concentration to 1. On the contrary, the model of Zhang et al. (1999) has a boundary condition, where the ice velocity towards the boundary is set to zero, otherwise the velocity is the average value of the velocities of adjacent pack ice points. At the ice/water boundary Zhang et al. (1999) treated the ice velocity correspondingly by setting the free drift velocity if directed away from the pack ice interior.

The ice strength parameter P^* was set to 1.5×10^4 N m^{-2}, which was considered to be the most representative for the ice edge zone in the Baltic Sea (Zhang Z., personal communication, 1999). Additionally, the ice model was run with several P^*s between 1.0×10^4 N m^{-2} and 2.0×10^4 N m^{-2}, but this did not change the outcome significantly.

4.1. Simulations

With the aid of the three different wind data sets, i.e., HIRLAM, MESAN, and the BASIS observations, the significance of the atmospheric forcing on sea-ice modelling was studied. The sea-ice velocities were simulated and then compared with the buoy observed drift.

Simulation cases:

1. Linear dependence (1) between the wind and the drift using the BASIS wind and the regression parameters of Table 1.
2. Routine forecast, with the operational FIMR ice model forced by HIRLAM winds. The forcing parameters were: $C_{a10}=1.8\times10^{-3}$, $C_w=3.5\times10^{-3}$ and $\xi=18°$. $\boldsymbol{u}_w$ was set to zero. These values were applied in operational model runs.
3. Same as case 2, but with the geostrophic winds derived from the MESAN air pressure fields. Atmospheric forcing parameters were: $C_g=3\times10^{-4}$ and $\phi=30°$. These values were obtained by fitting the $\boldsymbol{u}_a$ of the drifters and the $\boldsymbol{u}_g$ of MESAN according to (3a) in the least squares sense.
4. Same as case 2, but with the 10 m winds derived from the MESAN fields.
5. Same as case 2, but with the BASIS winds.
6. Same as case 5, but τ_a was calculated by including the stability effects (air temperatures at two levels), and the effects of ice floes (ice concentration and thickness).
7. Same as case 6, but the velocity of the open water buoy 7198 was substituted for $\boldsymbol{u}_w$ in (3b) to estimate the τ_w.

The atmospheric momentum flux was estimated according to (3a), and in cases 2 to 5 C_a was assumed to be a constant. In cases 6 and 7, C_a was not constant and depended on the stability of the atmospheric boundary layer and on the form drag due to ice floe edges (which can be estimated knowing the ice concentration and ice and snow thicknesses) following Uotila et al.

(2000). In cases 6 and 7 the geometrical roughness of the drifting ice floes was estimated to be 5 cm, resulting in a C_{aN10} of 1.46×10^{-3} (Banke et al., 1980). The atmospheric boundary layer was usually stably stratified, which decreased the mean C_{a10} to 1.3×10^{-3}. The stability information was obtained from the weather mast measurements at the Aranda site. The effect of ice floe edges increased the C_{a10} of 5893 and 9868 to about 1.4×10^{-3}. This effect may still be underestimated because of the omission of narrow leads and open water areas smaller than the resolution of the initial ice concentration fields.

The momentum flux time series in the cases 2 to 6 at the 5893 location are presented in Fig. 7. Because the momentum flux depends on the square of the wind speed, the deviation between the cases is especially large in high wind conditions. Case 5 seems to overestimate τ_a compared to the stability-dependent case 6. The MESAN-winds-based estimate (case 4) follows case 5 quite well, as would be expected from the high correlation between the BASIS and MESAN winds (see Subsection 2.3). Case 3 gives quite satisfactory estimates, but also deviates a lot from other estimates, as for example on 23 and 24 February. Case 2 has difficulties in following the other cases. For example, on 21 and 24 February the high wind conditions were not forecast by HIRLAM, resulting in too low τ_a estimates on these days.

Magnitudes of complex vector correlation coefficients (Kundu, 1976) and average velocity differences for the simulation cases are presented in Table 2 for the 3 buoys. Kundu (1976) defined the complex vector correlation coefficient as a normalized inner product

$$\langle w_1 w_2^* \rangle / (\langle w_1 w_1^* \rangle \langle w_2 w_2^* \rangle)^{1/2}$$

between two complex vector time series w_1 and w_2. Here the * denotes the complex conjugate and the $\langle\ \rangle$ represents an ensemble average. For the 18 km ice model only simulations 2 and 6 are presented in Table 2, marked as o2 and o6, because the mutual differences with the remaining cases were about the same as with the 5 km ice model.

The drift of buoy 5893 was highly wind-dependent with a correlation of 0.9. When the 5893 drift was modelled with the 18 km model (simulation o2 in Table 2), the correlation dropped to 0.5, and $\overline{\Delta V}$ between the modelled and observed velocities doubled. In this simulation the wind was underestimated, as was shown in Fig. 7. Additionally, the coarse grid of 18 km and the time step of 6 h were not fine enough to simulate the ice motion, and the sea surface currents were excluded. Simulation 2 with the 5 km model

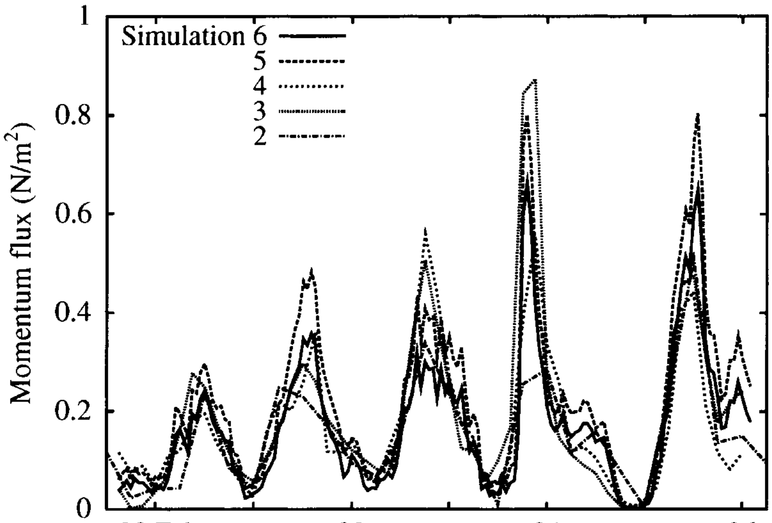

Fig. 7. Momentum flux time series for 5893 from the simulation cases.

Table 2. *Complex vector correlation coefficient magnitude (r) and the mean velocity difference ($\overline{\Delta V}$) between the observed and modelled drift velocities; simulations with the prefix "o" are model runs with the 18-km ice model, while the remainder are with the 5-km ice model; the correlation bounds are the 95% confidence limits of the coefficients. N gives the number of observations per simulation*

Buoy	Simulation	r	$\overline{\Delta V}$	N
5893	1	0.89 (0.92 … 0.85)	0.13	156
	o2	0.47 (0.58 … 0.33)	0.24	153
	2	0.72 (0.79 … 0.63)	0.20	156
	3	0.81 (0.86 … 0.75)	0.18	156
	4	0.82 (0.86 … 0.76)	0.19	156
	5	0.83 (0.87 … 0.77)	0.19	156
	o6	0.70 (0.77 … 0.60)	0.19	156
	6	0.87 (0.91 … 0.83)	0.17	156
	7	0.91 (0.93 … 0.88)	0.14	156
9868	1	0.75 (0.82 … 0.66)	0.11	121
	o2	0.50 (0.62 … 0.34)	0.11	114
	2	0.67 (0.73 … 0.61)	0.09	324
	3	0.74 (0.78 … 0.68)	0.08	324
	4	0.72 (0.77 … 0.66)	0.09	324
	5	0.82 (0.87 … 0.74)	0.09	121
	o6	0.42 (0.55 … 0.26)	0.12	121
	6	0.83 (0.88 … 0.76)	0.09	121
7199	1	0.59 (0.70 … 0.46)	0.11	121
	2	0.63 (0.73 … 0.51)	0.10	121
	3	0.62 (0.72 … 0.49)	0.10	121
	4	0.66 (0.75 … 0.54)	0.10	121
	5	0.67 (0.76 … 0.56)	0.10	121
	6	0.67 (0.76 … 0.55)	0.10	121

increased the correlation from 0.5 to 0.7, which is about as much as the increase of correlation by applying the 18 km model with the most correct wind forcing in simulation o6. Between simulations o6 and 6 the correlation increases from 0.7 to 0.9, which is (again) about the same as the increase achieved using the best wind forcing in simulation 6 compared to simulation 2. The velocity differences between the observed and modelled velocities $\overline{\Delta V}$ decreased by 0.03 ms^{-1} and by 0.02 ms^{-1}: compare simulations o2 and 2, and simulations o6 and 6, as the effect of the grid resolution increase. The enhanced wind forcing reduced $\overline{\Delta V}$ at least as much as the finer grid. The differences between simulations o2 and o6, and simulations 2 and 6 were 0.05 ms^{-1} and 0.03 ms^{-1}, respectively.

In simulation 3, the modelled velocity of buoy 5893 correlated more with the observations than in simulation 2, because the time step between the MESAN analyses was 3 hours and the MESAN analysis fields provided better forcing than the operational HIRLAM analyses and forecasts. There were no great differences between simulation 3 based on $\boldsymbol{u}_g$, and simulations 4 and 5, based on MESAN and BASIS surface winds. In simulation 6, the correlation increased practically to the same level as in simulation 1. This is expected to be the case, because the BASIS winds were utilized in both simulations 1 and 6. The relationship between the drift and the wind was close to linear, which is satisfied by simulation 1 and by the ice model. In addition, the parameters (scaling factor, turning angle and additive term) of simulation case 1 were statistically optimized for each drifter, which explains the relatively high correlation and small $\overline{\Delta V}$ when compared to those of the numerical ice model.

The probability that the correlation increased between simulation 5 (C_a was constant) and simulation 6 (C_a was not constant) was 96%. Thus a C_a depending on stability and ice conditions produces better coherence with the observed drift of 5893. However, $\overline{\Delta V}$ still remained almost as high as in simulation 2. This seemed to be due to the lack of the surface currents, because $\overline{\Delta V}$ in simulation 7 was about the same as in the simulation 1.

In simulations 2 to 6 $\boldsymbol{u}_w$ was set to zero, because no reliable current estimates were available for the analysis. The operational ice forecasts of FIMR were made with the same assumption. If the real $\boldsymbol{u}_w$ had been observed and had applied in the simulations, the differences between simulated $\boldsymbol{u}_i$ with various τ_a would have been smaller because $\boldsymbol{u}_i$ would have followed more $\boldsymbol{u}_w$. Therefore the comparisons by assuming the zero $\boldsymbol{u}_w$ produce greater differences between simulated ice velocities than the simulations with varying $\boldsymbol{u}_w$. The significance of $\boldsymbol{u}_w$ was demonstrated in simulation case 7, where the velocity of 7198 was used as a crude estimate. This case is presented for buoy 5893, because the inclusion of $\boldsymbol{u}_w$ only improved the modelled motion of this drifter.

The undrogued drift of 7198 and the drift of 5893 were compared with the sea level fluctuations in the Bothnian Bay. The hourly time series from Pietarsaari and Raahe stations (both at the Finnish coast) were averaged to provide the mean sea level in the Bothnian Bay and the resulting time series was filtered with 24 h Gaussian filter. The time difference of the filtered sea level time series was then compared with the buoy velocities, which were divided (i.e., rotated 50° clockwise from the north) along the coast and perpendicular to the coast components.

The correlations between the sea level fluctuations and the along coast components of the buoy velocities were calculated. The 7198 and 5893 along coast components and the sea level time difference correlated with the coefficients of 0.9. The high correlation reveals the high significance of the ocean current on the sea-ice motion in the central part of the basin. In addition, the high correlation between the open water drifter and the sea level fluctuations indicate that the undrogued open water drift at least roughly followed the sea surface current. The buoy velocities were also compared with the sea level gradient between the Bothnian Bay and the Bothnian Sea, but the resulted correlation coefficients were less than 0.6. The importance of the sea surface current for the 5893 drift is illustrated in Fig. 8, where the difference between simulations 6 and 7 is evident before 21 February and on 24 and 25 February. The inclusion of the current apparently improved the modelled speed. On 25 February the buoy speed was too high in simulation 7 and the velocity of 7198 no longer represented the current velocity of the region.

The difference between the velocity directions of simulations 6 and 7 (Fig. 8b) was not as apparent as that between the magnitudes. This may follow from the guiding effect of the basin's coast and the wind, when both the wind-dependent ice motion and the currents were forced to be in the same direction. There were still large deviations between the observed and modelled directions on 21 and 22 February, when the drift magnitude was weak. The observed rotational cycles lasted about 12 h, had a radius of about 750 m (see Fig. 3, the circle of 5893 on 21 February) and were probably inertial oscillations. The theoretical radius of the inertial circle is u_i/f. For a speed of 0.1 m/s it is less than 800 m in this area, which is below the resolution of the 5 km ice model. The buoy motion of 7199 and 9868 was also simulated by including the 7198 velocities as the current estimates, but this did not improve the modelled velocities. In addition, the correlations between the along coast velocities of 7199 and 9868 and the sea level fluctuations remained below 0.5.

Simulation 1 did not explain the drift near the coastline (buoys 9868 and 7199) as well as in the central basin (buoy 5893, Table 2). The 18 km model was not able to simulate the ice motion near the coastline because of its coarse grid. The correlation between the 18 km model and the observations was for 9868 0.5. The correlation was even worse for 7199 and was therefore not included in Table 2. The simulations of 7199 and 9868 are much more realistic with the 5 km model. By using any wind forcing from cases 2 to 6, the simulated velocities correlate equally well or better with the observations compared with simulation 1. When simulating 9868 drift, simulations 5 and 6, based on the BASIS wind, correlated better with the observed drift than simulations 2 to 4, based on HIRLAM or MESAN fields. By contrast, the differences between $\overline{\Delta V}$ in the corresponding simulations for 9868 were small. For 7199, no significant differences in correlation or $\overline{\Delta V}$ between the simulations were found.

Near the coast the initial fields of the ice concentration and thickness had more influence than the wind field. The initial ice field information resolution was about 18 km, and was not able to separate the narrow leads and channels of low ice concentration where the buoys may have been drifting at a relatively high speed. In some cases, such conditions were identified from RADARSAT images (see Subsection 2.1). Thus the best correlations achieved with the numerical model were about 0.8 and 0.7 for 9868 and 7199, respectively. In the central basin, the wind forcing and the wind-induced surface currents had more influence on ice motion, and the numerical model correlated with observations with a coefficient of 0.9.

In Fig. 9 the dependence between the simulated and observed sea ice speeds is presented. The free drift simulation was optimized for each buoy separately and provided the best linear fit between the wind and the drift in the least squares sense. Accordingly, the linear model overestimated low observed speeds and underestimated high observed ones (Fig. 9a). When the 18 km model was applied, the coastal fast-ice zone caused the low modelled speed to be roughly as small as that observed, but the deviation was very high (Fig. 9b). In particular, the simulated speed was often zero, while the observed speed was high, which was due

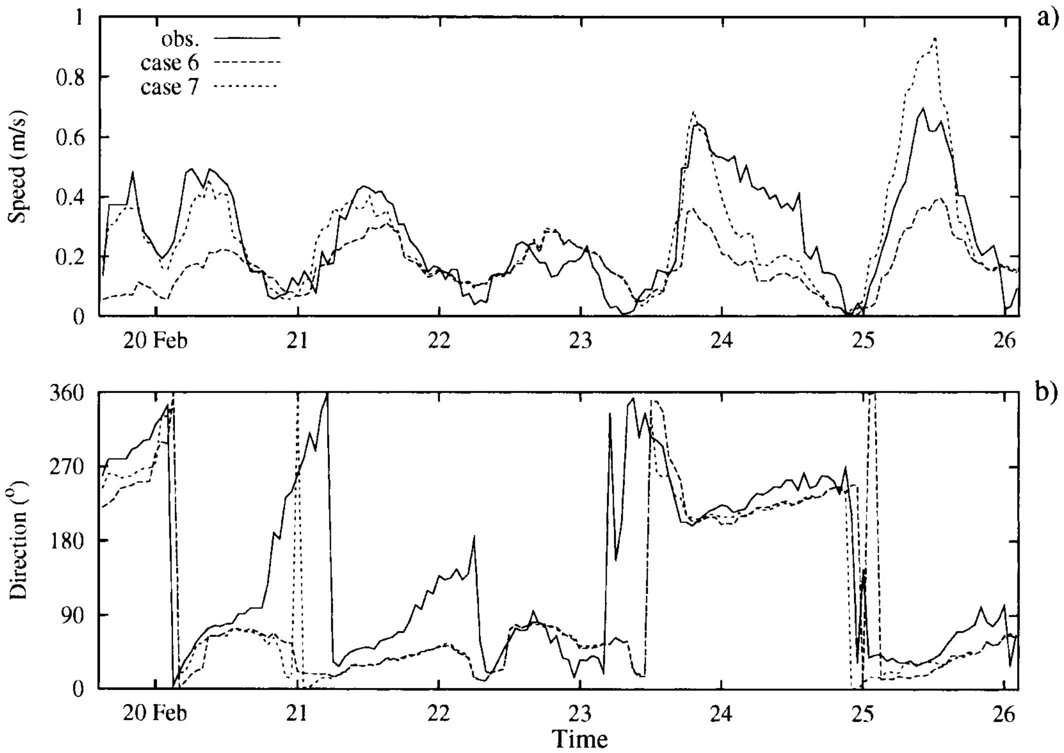

Fig. 8. Comparison of the observed drift and the (a) speed and (b) direction of buoy 5893 in the simulation cases 6 and 7.

to the coarse resolution of the model near the fast ice zone. The situation improved when the ice model resolution was increased to 5 km (Fig. 9c). There were cases when the ice model resulted in too high or too low speeds because of erroneous wind forecasts, and the modelled speed approached that observed by using the most sophisticated wind forcing of simulation 6 and the surface current estimate of simulation 7 (Fig. 9d). Finally, there remained cases in which the ice condition information was incorrect due to the coarse input fields, resulting in lower modelled speeds than those observed.

5. Conclusions

The ice motion was primarily driven by the wind and the changing wind directions, and the ice mainly drifted along-shore or seaward. When the wind forced ice towards the fast ice zone, the pack ice moved slowly or was stuck near the coast. The internal ice stress became important and the motion of the buoys in the shear zone was only explained by the high-resolution numerical ice model including more realistic ice rheology. In moving pack ice, where the ice concentration was low, the ice motion was well explained by assuming a linear relationship between the wind and the drift. This is a physically valid relationship when thin ice drifts freely in steady-state conditions.

Occasionally the buoys moved at a relatively high speed near the coast, although the ice concentration derived from the ice charts was high. The modelled ice speeds were too low due to the high concentration of the input fields. In these cases it seemed that the buoys drifted in leads of low ice concentration. These openings were too narrow to be seen in the initial ice condition fields and the buoy drift did not represent the average ice motion in a model grid square.

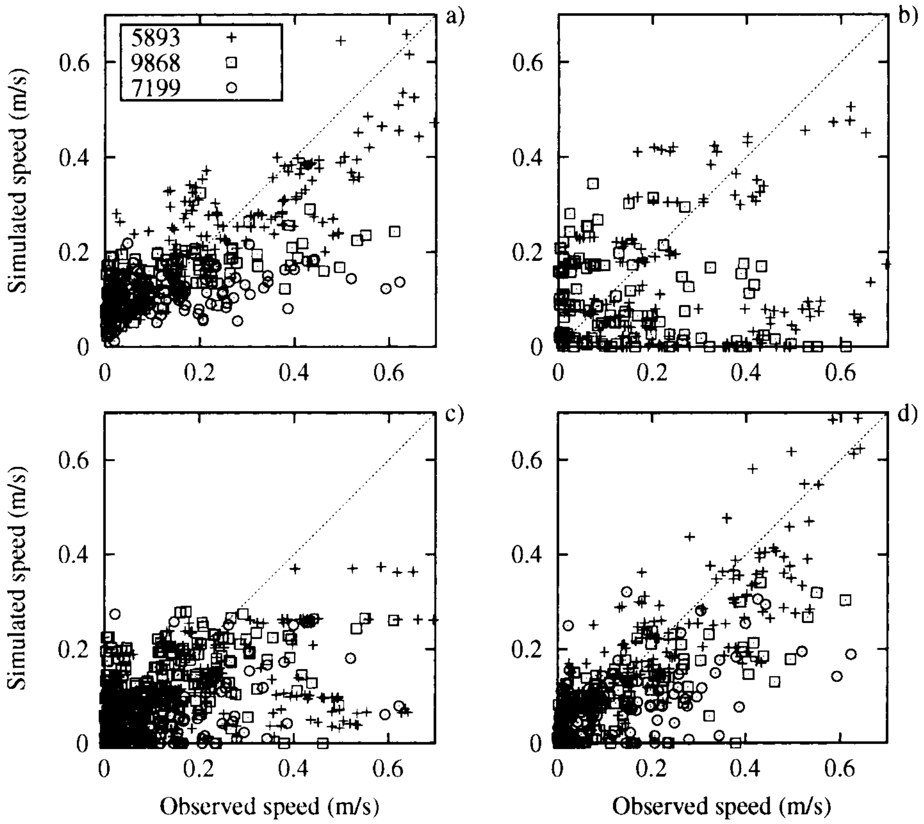

Fig. 9. Relations between the observed (horizontal axis) and simulated speed (vertical) in (a) simulation 1, (b) simulation o2, (c) simulation 2, and (d) simulation 6 for buoys 7198 and 9868, and in simulation 7 for buoy 5893. The simulation o2 is the model run with the 18-km ice model, while the remainders are with the 5-km ice model.

The drifting ice responded most apparently to the wind at periods longer than 7 h. Near the fast ice the wind-drift coherence was significant over a narrower frequency range than further away from the coast. In addition, the kinetic energy of the ice motion was highest at periods of about one to two days, because the dimensions of the basin restricted the drift at longer periods. The open water drifter velocity was coherent with the wind at periods longer than 30 h, but also the periods near the inertial frequency. In addition, one ice buoy displayed inertial circles when the wind speed and the ice concentration were small. The radius of the circles was below the resolution of the 5 km ice model, which did not resolve the motion.

The significance of the sea surface currents on the open pack ice drift was apparently revealed by the sea level fluctuations. The sea level time difference in the Bothnian Bay had the highest correlation with the buoy drift, while the sea level gradient between the Bothnian Sea and Bothnian Bay corresponded to the buoy speeds only during the strongest in/outflow events. The weak similarity of the sea level gradient and the observed buoy motion seem to support the conclusion that the water exchange between the basins was relatively small during the study period. However, the buoy trajectories reveal that the ice drifted from the northern Bothnian Sea to the Bothnian Bay thus transporting heat between the basins.

The scaling factor between the ice and the wind was relatively high in the centre of the basin because the ice was driven by the wind-induced sea surface current in addition to the direct wind stress on the ice surface. Accordingly, the ice motion was well modelled by applying the surface current estimate. While surface currents are not routinely measured, the necessity of a coupled ice-ocean model is apparent for solving the ice motion.

Winds derived from MESAN fields proved to provide accurate forcing to the ice drift. By using the most correct wind forcing compared to the wind applied in the operational model, the modelled ice velocities in the drifting pack ice were improved as much as by replacing the 18 km model by the 5 km one. In addition, the modelled drift clearly approached the observed drift when C_a was assumed to be dependent on the atmospheric stability and ice conditions in contrast to using a constant C_a. Near the fast ice the inclusion of the surface current and a non-constant C_a did not improve the modelled drift. The calculation of momentum flux following Uotila et al. (2000) can easily be included in a coupled atmosphere-ice model with information on the atmospheric surface layer stratification, ice concentration, and ice and snow thickness.

6. Acknowledgements

I wish to thank Zhanhai Zhang for allowing the use of his ice model for this study. Bertil Håkansson and Maria Lundin from SMHI are acknowledged for providing the MESAN analysis, SMHI digitized ice charts and the SMHI BASIS field data. Heinrich Hoeber from the University of Hamburg and Ann-Sofie Smedman from Uppsala University are acknowledged for providing their BASIS field measurements. The BASIS group of FIMR is gratefully acknowledged. Jouko Launiainen and Timo Vihma particularly are thanked for project co-operation, and discussions and comments on the manuscript. Jouni Vainio and Bin Cheng kindly assisted me with the operational FIMR ice model and the FMI HIRLAM fields. This study is part of the EC-funded project BALTEX-BASIS carried out under contract MAS3-CT97-0117.

REFERENCES

Banke, E. G., Smith S. D. and Anderson R. J. 1980. Drag coefficients at AIDJEX from sonic anemometer measurements. In: *Sea ice processes and models*, edited by R. S. Pritchard, pp. 430–442. Univ. of Washington Press, Seattle, U.S.A.

Geiger, G. A., Hibler W. D. III, and Ackley S. F. 1998. Large-scale sea ice drift and deformation: comparison between models and observations in the western Weddell Sea during 1992, **103**, 21,893–21,913.

Gonella, J. 1972. A rotary-component method for analysing meteorological and oceanographic vector time series. *Deep-Sea Res.* **19**, 833–846.

Gustafsson, N., Nyberg L. and Omstedt A. 1998. Coupling of a high-resolution atmospheric model and an ocean model for the Baltic Sea. *Mon. Wea. Rev.* **126**, 2822–2846.

Häggmark, L., Ivarsson K.-I., Gollvik, S. and Olofsson, P.-O. 2000. Mesan, an operational mesoscale analysis system. *Tellus* **52A**, 2–20.

Hansen, D. V. and Herman, A. 1989. Temporal sampling requirements for surface drifting buoys in the tropical Pacific. *J. Atmos. and Oceanic Technol.* **6**, 599–607.

Hansen, D. V. and Poulain, P.-M. 1996. Quality control and interpolations of WOCE-TOGA drifter data. *J. Atmos. and Oceanic Technol.* **13**, 900–909.

Hibler, W. D. III, 1979. A dynamic thermodynamic sea ice model. *J. Phys. Oceanogr.* **9**, 815–846.

Hibler, W. D. III and Schulson, E. M. 1997. On modeling sea-ice fracture and flow in numerical investigations of climate. *Annals of Glaciology* **25**, 26–32.

Kottmeier, C. and Sellmann, L. 1996. Atmospheric and oceanic forcing of Weddell Sea ice motion. *J. Geophys. Res.* **101**, 20,809–20,824.

Kundu, P. K. 1976. Ekman veering observed near the ocean bottom. *J. Phys. Oceanogr.* **6**, 238–242.

Launiainen, J. (ed.), 1999. BALTEX-BASIS Data Report 1998. *International BALTEX Secreteriat, publication no. 14*, 94 pp.

Leppäranta, M. 1981. An ice drift model for the Baltic Sea. *Tellus* **33**, 583–596.

Leppäranta, M. and Omstedt, A. 1990. Dynamic coupling of sea ice and water for an ice field with free boundaries. *Tellus* **42A**, 482–495.

Leppäranta, M. and Zhang, Z. 1992. A viscous-plastic ice dynamics test model for the Baltic Sea. *Finnish Inst. of Marine Res.*, internal report, 3.

Leppäranta, M., Sun, Y. and Haapala, J. 1998. Comparisons of sea-ice velocity fields from ERS-1 SAR and a dynamic model. *J. Glaciology* **147**, 248–262.

Martinson, D. G. and Wamser, C. 1990. Ice drift and momentum exchange in winter Antarctic pack ice. *J. Geophys. Res.* **95**, 1741–1755.

Omstedt, A. 1990. Modelling the Baltic Sea as 13 subbasins with vertical resolution. *Tellus* **42A**, 286–301.

Omstedt, A., Nyberg, L. and Leppäranta, M. 1996. On the ice–ocean response to wind forcing. *Tellus* **48A**, 593–606.

Thomas, D. 1999. The quality of sea ice velocity estimates. *J. Geophys. Res.* **104**, 13,627–13,652.

Thorndike, A. S. and Colony, R. 1982. Sea ice motion in response to geostrophic winds.*J. Geophys. Res.* **87**, 5845–5852.

Uotila, J., Launiainen, J. and Vihma, T. 1995. Analysis of the surface drift currents in the Bothnian Sea. *Geophysica* **31**, 37–49.

Uotila, J., Vihma, T. and Launiainen, J. 2000. Response of the Weddell Sea pack ice to wind forcing. *J. Geophys. Res.* **105**, 1135–1151.

Vihma, T., Launiainen, J. and Uotila, J. 1996. Weddell Sea ice drift: kinematics and wind forcing. *J. Geophys. Res.* **101**, 18,279–18,296.

Zhang, J. and Hibler, W. D. III, 1997. On an efficient numerical method for modeling sea ice dynamics. *J. Geophys. Res.* **102**, 8691–8702.

Zhang, Z. H., Leppäranta, M., Haapala, J. and Stipa, T. 1999. Numerical simulation of sea ice drift in the Bay of Bothnia. *POAC'99 Proceedings.* Helsinki University of Technology, Espoo, Finland, pp. 488–496.